

Dalton Transactions

Accepted Manuscript



This is an *Accepted Manuscript*, which has been through the Royal Society of Chemistry peer review process and has been accepted for publication.

Accepted Manuscripts are published online shortly after acceptance, before technical editing, formatting and proof reading. Using this free service, authors can make their results available to the community, in citable form, before we publish the edited article. We will replace this *Accepted Manuscript* with the edited and formatted *Advance Article* as soon as it is available.

You can find more information about *Accepted Manuscripts* in the [Information for Authors](#).

Please note that technical editing may introduce minor changes to the text and/or graphics, which may alter content. The journal's standard [Terms & Conditions](#) and the [Ethical guidelines](#) still apply. In no event shall the Royal Society of Chemistry be held responsible for any errors or omissions in this *Accepted Manuscript* or any consequences arising from the use of any information it contains.

Ag₂S/g-C₃N₄ Composite Photocatalysts for Efficient Pt-free Hydrogen Production. The Co-catalyst Function of Ag/Ag₂S Formed by Simultaneous Photodeposition

Deli Jiang*, Linlin Chen, Jimin Xie, and Min Chen*

School of Chemistry and Chemical Engineering, Jiangsu University, Zhenjiang 212013, China

* Corresponding author:

E-mail address: dlj@ujs.edu.cn, chenmin3226@sina.com.

Abstract: Without Pt as cocatalysts, the photocatalytic hydrogen evolution activity of graphitic carbon nitride (g-C₃N₄) or even their composite is normally rather low (<1 μmol h⁻¹). Exploring a Pt-free cocatalysts to substitute precious Pt is of great importance in the photocatalytic field. In the present work, Ag₂S-modified g-C₃N₄ (Ag₂S/g-C₃N₄) composite photocatalysts were prepared via a simple precipitation method. The results demonstrated that, the photocatalytic H₂-production activity of g-C₃N₄ can be remarkably increased by the combination of Ag₂S. The optimal Ag₂S loading was found to be 5 wt%, giving a H₂ production of 10 μmol h⁻¹, around 100 times that of pure g-C₃N₄. The enhanced photocatalytic activity can be mainly attributed to the effective charge transfer between g-C₃N₄ and Ag/Ag₂S, of which latter is formed by simultaneous photodeposition in the photocatalytic H₂ evolution reaction and acts as an efficient co-catalyst for the g-C₃N₄. This work showed the possibility for the utilization of Ag₂S or Ag/Ag₂S a substitute for Pt in the photocatalytic H₂ production using g-C₃N₄.

1. Introduction

The increasing demands for the production of energy have led to the search for renewable alternative energy resources. Photocatalytic hydrogen production using semiconductor particles has been regarded as one of the most promising means of clean energy production from renewable sources since its discovery by Honda and Fujishima in 1972.¹ To date, various semiconductor photocatalysts have been developed for the production of H₂, including oxides,²⁻⁴ sulfides,^{5,6} oxynitrides^{7,8} and nanocomposites.⁹⁻¹¹ As a metal-free semiconductor photocatalyst, graphite-like carbon nitride (g-C₃N₄) has attracted more and more attentions owing to its suitable band position and stable, low-cost characteristics.¹² Nevertheless, some inherent drawbacks of g-C₃N₄ such as the deficient sunlight absorption (below the wavelength of 460 nm), low surface area, the high recombination rate of photogenerated charges largely limit the photocatalytic hydrogen evolution activity.^{13,14} Enormous attempts have been dedicated to improve the photocatalytic performance of g-C₃N₄, such as nanostructuring,¹⁵⁻¹⁸ doping,¹⁹⁻²² copolymerization,²³⁻²⁵ and cocatalyzing.²⁶⁻³³ Although great success have been achieved for enhancement of photocatalytic hydrogen evolution activity of g-C₃N₄, it should be noted that without Pt performing as cocatalysts, the activity of g-C₃N₄ or even their modified composite is normally rather low (<1 μmol h⁻¹).^{12,34-36} Pt is a rare and expensive noble metal, which is the main obstacle for large scale application of such noble metal in photocatalysis. Therefore, it is of both scientific and economic importance to investigate alternative low cost Pt-free cocatalysts.

In recent years, metal sulfides nanoparticles such as Cd- or Pb-based metal sulfides nanoparticles have received great interest in the construction of composite photocatalysts owing to their narrow band gaps and high quantum efficiency.^{5,37} Wang and co-workers have recently

reported the synthesis of earth-abundant MoS₂/g-C₃N₄ layered heterojunctions, of which MoS₂ functions as co-catalysts for the g-C₃N₄.³⁸ These junctions exhibited enhanced photocatalytic H₂-evolution activity under visible-light irradiation, and their performance was comparable to that of Pt/g-C₃N₄. Very recently, Xu and co-workers found that the photocatalytic hydrogen-evolution activity of g-C₃N₄ can be greatly enhanced (towards 250 times) by loading NiS nanoparticles as cocatalyst.³⁹ However, such efficient Pt-free co-catalysts are very limited. Therefore, development of an effective co-catalyst for g-C₃N₄ photocatalytic H₂ production is required.

Silver sulfide (Ag₂S), as a direct semiconductor with narrow-band gap of 1.1 eV, has a relatively large absorption coefficient, leading to its wide applications in photovoltaic cells, photocatalytic applications.⁴⁰⁻⁴⁶ Here, for the first time, we demonstrate the synthesis of Ag₂S/g-C₃N₄ composite photocatalyst by a simple facile precipitation route, and their visible light-driven photocatalytic H₂ production activity from aqueous solutions containing methanol without Pt cocatalyst. The results show that Ag₂S/g-C₃N₄ composite exhibits significantly improved photocatalytic H₂ production compared with that of pristine g-C₃N₄. The effect of the Ag₂S/g-C₃N₄ weight ratio on the photocatalytic H₂ production activity was investigated, and a probable mechanism of the enhanced photoactivity was discussed. This work highlights the utilization of Ag₂S or Ag/Ag₂S as a substitute for Pt in the photocatalytic H₂ production using g-C₃N₄.

2. Experimental section

2.1 Sample preparation

The g-C₃N₄ was synthesized by thermal treatment of 10 g of urea in a crucible with a cover under ambient pressure in air. After dried at 80 °C for 24 h, the precursor was heated to 550 °C at

a heating rate of 2.3 °C /min in a tube furnace for 4 h in air. The resulted final light yellow powder were washed with nitric acid (0.1 mol/L) twice, deionized water and absolute ethanol three times, and then dried at 60 °C for 12 h.

Ag₂S/g-C₃N₄ composite photocatalysts were prepared by in situ growth of Ag₂S on g-C₃N₄ surface at room-temperature. Typically, 0.092 g of g-C₃N₄ powders and different amounts of AgNO₃ were dispersed in 50 mL absolute ethanol in a 100 mL beaker. After ultrasonication for 20 min, a certain amount of thioacetamide (TAA) was added into the mixture with subsequent stirring. After stirring for 4h, the product was collected by centrifugation, washed with distilled water and absolute ethanol, and dried in an oven at 60 °C for 12h. According to this method, different weight ratios of the Ag₂S to g-C₃N₄ samples were obtained and labeled as 1% Ag₂S/g-C₃N₄, 2% Ag₂S/g-C₃N₄, 5% Ag₂S/g-C₃N₄, and 10% Ag₂S/g-C₃N₄, respectively. Pure Ag₂S was also synthesized for comparison purpose in the absence of g-C₃N₄. For comparison purpose, a 1.0 wt% Pt/g-C₃N₄ sample was synthesized by photoreduction process. Typically, a certain amount of H₂PtCl₆ was added into the g-C₃N₄ suspension. Next, the suspension was stirred and irradiated (300W Xe arc lamp) for 30 min at room temperature to reduce the Pt species.

2.2 Characterization

The phase purity and crystal structure of the obtained samples were examined by X-ray diffraction (XRD) using D8 Advance X-ray diffraction (Bruker axs company, Germany) equipped with Cu-KR radiation ($\lambda=1.5406 \text{ \AA}$), employing a scanning rate of 7° min^{-1} in the 2θ range from 10 to 80° . Infrared spectra were obtained on KBr pellets on a Nicolet NEXUS470 FTIR in the range of $4000\text{--}500 \text{ cm}^{-1}$. Surface analysis of the sample was examined by X-ray photoelectron spectroscopy (XPS) using a ESCA PHI500 spectrometer. Transmission electron microscopy (TEM)

was recorded on a JEOL-JEM-2010 (JEOL, Japan) operating at 200 Kv. The Ag₂S contents in the composites were analyzed by inductively coupled plasma spectroscopy (ICP, Optima2000DV, USA) analysis. UV–vis diffuse reflectance spectra (DRS) were recorded on a Shimadzu UV-2401 spectrophotometer equipped with spherical diffuse reflectance accessory. The Brunauer–Emmett–Teller (BET) specific surface area and pore size distribution of the samples were characterized by nitrogen adsorption with Tristar II 3020 instrument. The photoluminescence (PL) spectra of the photocatalyst were obtained by a Varian Cary Eclipse spectrometer with an excitation wavelength of 330 nm.

2.3 Photocatalytic hydrogen production

The photocatalytic hydrogen production experiments were performed in a 100 mL Pyrex flask at ambient temperature and atmospheric pressure, and the openings of the flask were sealed with silicone rubber septums. Four low power UV-LEDs (3 W, 420 nm) (Shenzhen LAMPLIC Science Co. Ltd. China), which were positioned 1 cm away from the reactor in four different directions, were used as light sources to trigger the photocatalytic reaction. The focused intensity and areas on the flask for each UV-LED was ca. 80.0 mW cm⁻² and 1 cm², respectively. In a typical photocatalytic experiment, 50 mg of photocatalyst was suspended in 80 mL mixed solution of methanol (20 mL) and water (60 mL). Prior to irradiation, the suspension of the catalyst was dispersed by an ultrasonic bath for 10 min, and then bubbled with nitrogen through the reactor for 40 min to completely remove the dissolved oxygen and ensure the reactor was in an anaerobic condition. A continuous magnetic stirrer was applied at the bottom of the reactor in order to keep the photocatalyst particles in suspension status during the whole experiments. A 0.4 mL gas was intermittently sampled through the septum, and hydrogen was analyzed by gas chromatography

(GC-14C, Shimadzu, Japan, TCD, with nitrogen as a carrier gas and 5 Å molecular sieve column).

3. Results and Discussion

3.1 Phase structures and morphology

Fig. 1 shows the XRD patterns of $\text{Ag}_2\text{S}/\text{g-C}_3\text{N}_4$ composites, as well as the pure $\text{g-C}_3\text{N}_4$ and Ag_2S samples. Two distinct diffraction peaks at 13.04 and 27.47 in the $\text{g-C}_3\text{N}_4$ sample, corresponding to the in-plane structural packing motif and interlayer stacking of aromatic segments, can be indexed as the (100) and (002) peaks for graphitic materials, respectively.^{19,32} These two peaks decrease in intensity gradually with the increase of introduced Ag_2S , suggesting that Ag_2S nanoparticles have been successfully loaded onto the surface of $\text{g-C}_3\text{N}_4$. For Ag_2S , all of the peaks in the XRD patterns matched well with the acanthite Ag_2S (space group $P21/n$), and the calculated lattice constants were $a = 4.226 \text{ \AA}$, $b = 6.928 \text{ \AA}$, and $c = 7.858 \text{ \AA}$ (JCPDS 14-0072). All the $\text{Ag}_2\text{S}/\text{g-C}_3\text{N}_4$ samples exhibit diffraction peaks corresponding to both $\text{g-C}_3\text{N}_4$ and acanthite Ag_2S , and no other impure peaks can be observed, suggesting a two-phase composition of $\text{g-C}_3\text{N}_4$ and Ag_2S in these composites.

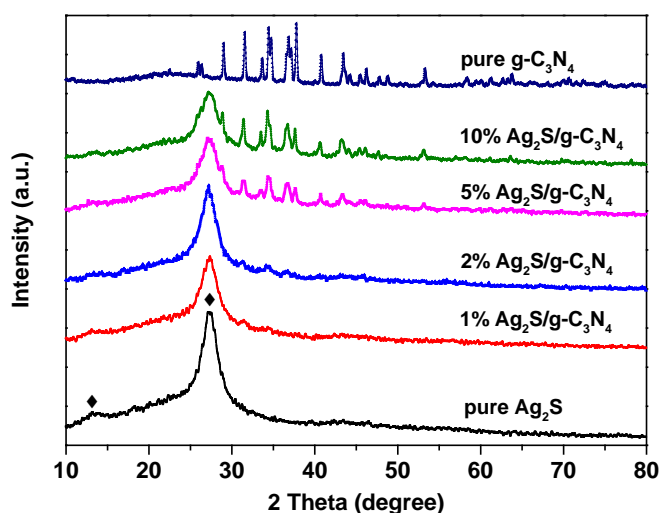


Fig. 1 XRD patterns of $\text{Ag}_2\text{S}/\text{g-C}_3\text{N}_4$ composites, $\text{g-C}_3\text{N}_4$, and Ag_2S samples.

The composition of $\text{Ag}_2\text{S}/\text{g-C}_3\text{N}_4$ composites was further characterized by FT-IR spectroscopy and the results were shown in Fig. 2. In the FT-IR spectrum of $\text{g-C}_3\text{N}_4$, the peaks at 1637 cm^{-1} are attributable to C=N stretching vibration modes, while the 1252 , 1323 and 1407 cm^{-1} can be ascribed to aromatic C-N stretching vibration modes.^{36,47} The peak at 810 cm^{-1} is related to characteristic breathing mode of triazine units.⁴⁸ The broad band centered at 3188 cm^{-1} can be assigned to the stretching mode of the N-H bond. It could also be clearly seen that the main characteristic peaks of $\text{g-C}_3\text{N}_4$ appeared in $\text{Ag}_2\text{S}/\text{g-C}_3\text{N}_4$ photocatalysts, suggesting that no structural change of $\text{g-C}_3\text{N}_4$ occurs during the hybridization process. With regard to the pure Ag_2S synthesized in the presence of TAA, the peaks at 1400 , 1643 , 3132 and 3454 cm^{-1} may be ascribed to the TAA on the surface of Ag_2S .⁴⁹

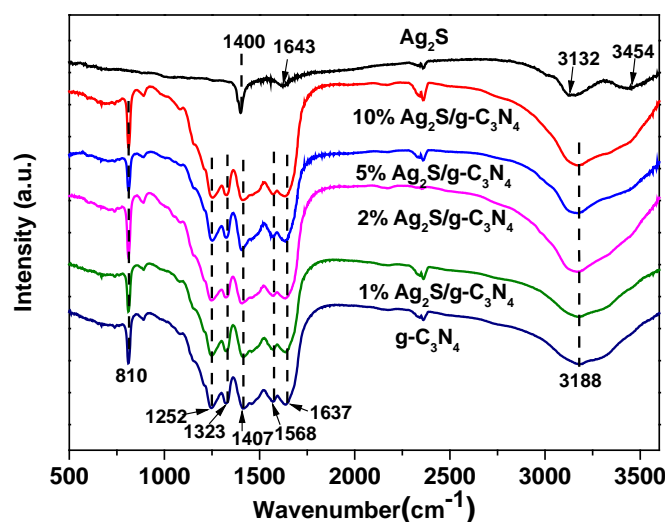


Fig. 2 FTIR spectra of $\text{g-C}_3\text{N}_4$, Ag_2S and $\text{Ag}_2\text{S}/\text{g-C}_3\text{N}_4$ samples.

XPS analyses were carried out on a typical 5% $\text{Ag}_2\text{S}/\text{g-C}_3\text{N}_4$ sample to evaluate the chemical valence state of the elements. The high resolution XPS spectra of C 1s shows that there were two peaks located at 284.6 and 288.3 eV. The peak centered at 284.8 eV can be assigned to the adventitious hydrocarbon from the defect-containing sp^2 -hybridized carbon atoms present in

graphitic domains, corresponding to a C-N-C coordination, while the peak centered at 288.3 eV was assigned to N-C=N₂ coordination.^{26,50} In the N 1s spectrum (Fig. 3b), several binding energies can be separated. The main signal showed occurrence of C-N-C groups (398.8 eV), tertiary nitrogen N-(C)₃ groups (399.8 eV) and N-H groups (401.0 eV). The peak at 404.9 eV could be related to the charging effects.^{51,52} Fig. 3c showed the peaks at 367.8 and 373.8 eV, which could be respectively attributed to Ag 3d_{5/2} and Ag 3d_{3/2} binding energies of Ag^I.⁵² The minor peaks of S 2p_{3/2} and S 2p_{1/2}, which were located at around 161.1 and 162.8 eV (Fig. 3d) were assigned to sulfur anions in the lattice of Ag₂S, correspondingly. Evidently, results from XRD, FT-IR and XPS revealed that the obtained composites contained g-C₃N₄ and Ag₂S.

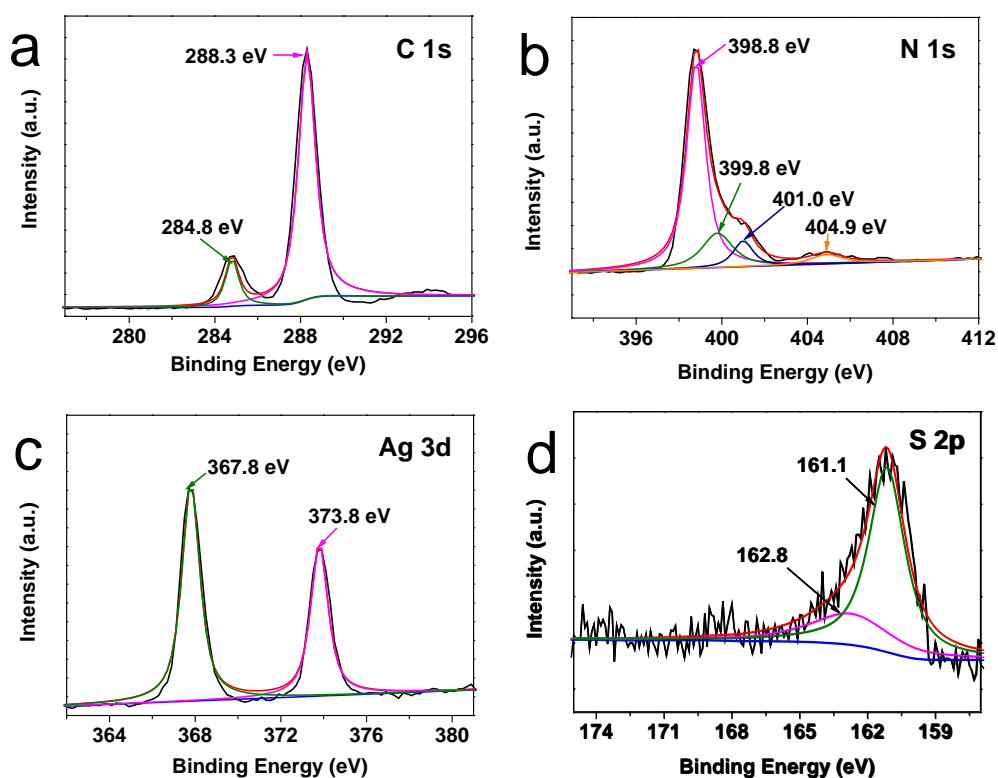


Fig. 3 XPS spectra of (a) C 1s, (b) N 1s, (c) Ag 3d and (d) S 2p of sample 5% Ag₂S/g-C₃N₄.

The morphology and microstructure of the Ag₂S/g-C₃N₄ composites was then investigated by TEM. Fig. 4a shows that a number of mesopores of several tens of nanometres in size can be

observed in the $g\text{-C}_3\text{N}_4$ sheets, which serve as a support to bound Ag_2S particles in this composite system. The TEM image for 1% $\text{Ag}_2\text{S}/g\text{-C}_3\text{N}_4$ sample shows that a few of Ag_2S nanoparticles with sizes approximately ranging from 8 to 16 nm were deposited on the surface of $g\text{-C}_3\text{N}_4$ sheets (Fig. 4b). As shown in Fig. 4c-e, for 2, 5, 10% $\text{Ag}_2\text{S}/g\text{-C}_3\text{N}_4$ sample, Ag_2S nanoparticles with increasing amounts were uniformly distributed on $g\text{-C}_3\text{N}_4$ sheet, no apparent aggregation of the Ag_2S nanoparticles was discerned which leads to the formation of interfaces between Ag_2S and $g\text{-C}_3\text{N}_4$. The morphology of pure Ag_2S was also shown in Fig. 4f, which indicates that Ag_2S has large particle size. The mass percentage of $\text{Ag}_2\text{S}/g\text{-C}_3\text{N}_4$ was determined by ICP analysis and the results show that the actual Ag_2S contents in the $\text{Ag}_2\text{S}/g\text{-C}_3\text{N}_4$ are 1.18%, 2.02%, 4.41%, and 9.22% for the 1%, 2%, 5%, and 10% $\text{Ag}_2\text{S}/g\text{-C}_3\text{N}_4$ samples, respectively.

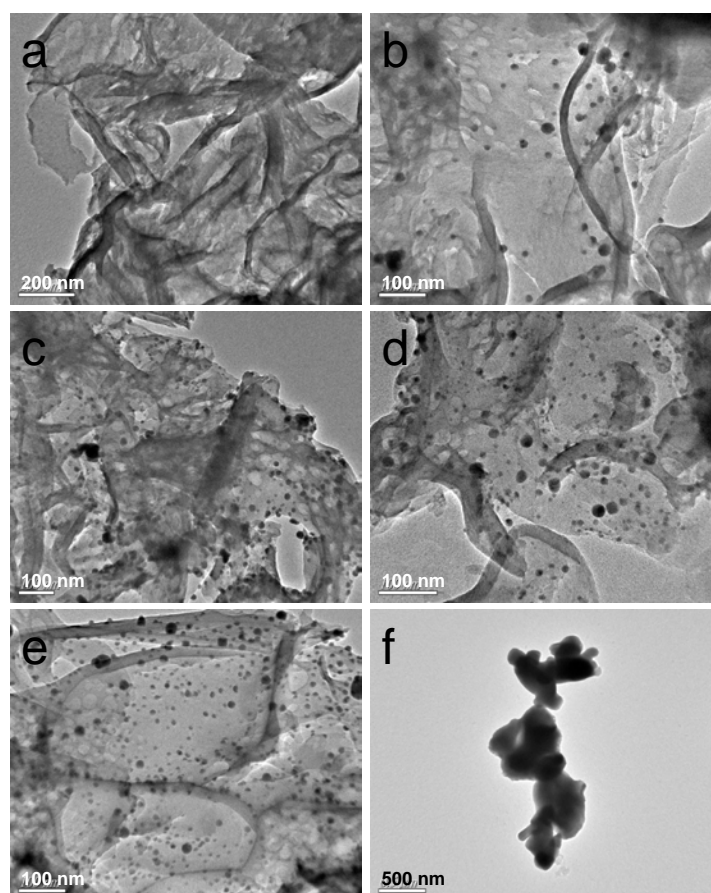


Fig. 4 TEM images of (a) pure $g\text{-C}_3\text{N}_4$, (b) 1% $\text{Ag}_2\text{S}/g\text{-C}_3\text{N}_4$, (c) 2% $\text{Ag}_2\text{S}/g\text{-C}_3\text{N}_4$, (d) 5%

Ag₂S/g-C₃N₄, (e) 10% Ag₂S/g-C₃N₄ and (f) pure Ag₂S.

3.2 N₂-Sorption studies

It is well-known that photocatalysts with higher specific surface areas and bigger pore volumes are beneficial for the enhancement of photocatalytic performance due to there being more surface active sites for the adsorption of reactant molecules, ease of transportation of reactant molecules and products through the interconnected porous networks, and enhanced harvesting of light.⁵³ Fig. 5 shows nitrogen adsorption-desorption isotherms and the corresponding pore size distribution curves of the as-prepared Ag₂S/g-C₃N₄ and pure g-C₃N₄ samples. The nitrogen adsorption-desorption isotherms of all samples are of type IV with a H3 hysteresis loop according to the IUPAC classification, reflecting the presence of a mesoporous structure of the composites (about 8-50 nm), which is well consistent with the TEM results. Tabel S1 summaries the BET surface areas and pore volumes of the samples. One can find that the BET surface areas of almost all the composite samples are slightly lower than pure g-C₃N₄. It is easy to understand that once Ag₂S nanoparticles deposit on the surface of g-C₃N₄ particles or embedded in the pores, they will reduce the specific surface area of the samples.

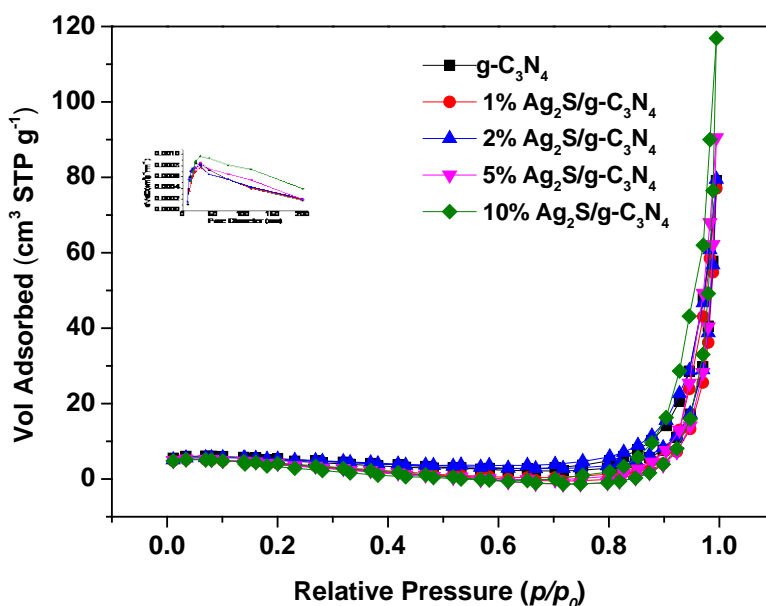


Fig. 5 Nitrogen sorption isotherm and Barrett–Joyner–Halenda (BJH) pore size distribution plot (inset) of the as-prepared samples.

3.3 UV-Vis diffuse reflection spectra

The light absorption properties of the pure $\text{g-C}_3\text{N}_4$, Ag_2S , and $\text{Ag}_2\text{S/g-C}_3\text{N}_4$ composites were characterized by UV-vis diffuse reflectance spectroscopy. As shown in Fig. 6, the $\text{g-C}_3\text{N}_4$ sample has the absorption edge of around 460 nm. The weak and broadened peaks centered at about 775 nm are similar to the reported UV-vis spectra of Ag_2S , which was accordance to the UV-vis spectra of pure Ag_2S .⁵⁴ The absorption edge of $\text{Ag}_2\text{S/g-C}_3\text{N}_4$ composites ranges from 460 to 490 nm. The absorption edges of the composites samples shifted to longer wavelengths as the amount of Ag_2S increased. The band gap energy of a semiconductor was calculated by this equation:

$$\alpha h\nu = A(h\nu - E_g)^{n/2} \quad (1)$$

Where α , h , ν , A and E_g are absorption coefficient, light frequency, and band gap, respectively.⁵⁵ Among them, n is determined from the type of optical transition of a semiconductor ($n = 1$ for direct transition and $n = 4$ for indirect transition. As previous literature reported, the n values of $\text{g-C}_3\text{N}_4$ and Ag_2S were 4 and 1 respectively.^{32,56} After calculated experimental data, E_g

of g-C₃N₄ was determined from a plot of $(\alpha h\nu)^{1/2}$ versus energy ($h\nu$), and the band gap energy of g-C₃N₄ is approximate 2.69 eV (Fig. S1a). Accordingly, E_g of Ag₂S was found to be 0.97 eV according to a plot of $(\alpha h\nu)^2$ versus energy ($h\nu$) (Fig. S1b). All the band gap values of g-C₃N₄ and Ag₂S were very close to previously reported results.^{12,54}

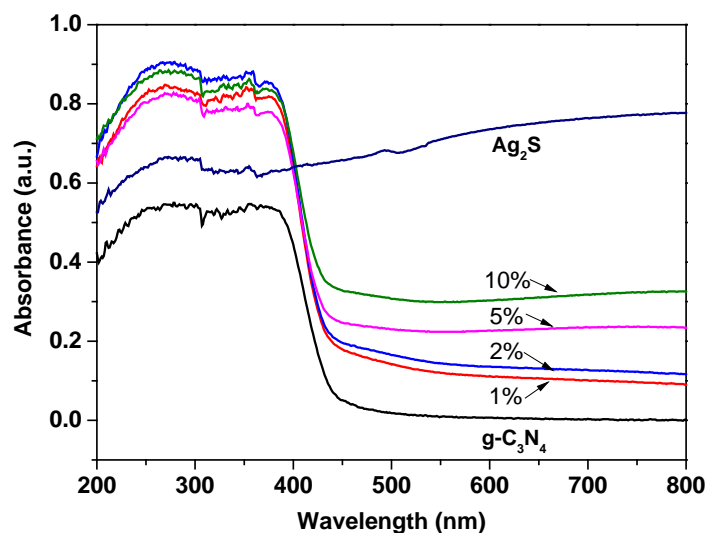


Fig. 6 UV-vis diffuse reflectance spectras of pure Ag₂S, C₃N₄ and the Ag₂S/g-C₃N₄ composites.

3.4 Photocatalytic H₂-production activity

The H₂ evolution experiments were performed by taking 50 mL of a 25 vol% methanol solution and 0.05 g of powdered photocatalyst. Before the actual photocatalytic experiment was performed, reference experiments were performed by taking a pure methanol solution in the absence of either photocatalyst or irradiation. No appreciable amount of H₂ was detected, which suggests that H₂ was produced from the methanol solution by photocatalytic reactions on photocatalyst. The influence of different Ag₂S contents in the Ag₂S/g-C₃N₄ composites on the H₂ evolution is presented in Fig. 7. It was found that pure g-C₃N₄ prepared from urea shows a negligible visible light H₂-production activity, although it could absorb visible light because of its 2.69 eV bandgap. This is probably due to the rapid recombination between electrons and holes,

and the fast backward reaction.³⁰ In contrast, after loading only 1 wt% Ag₂S, the H₂ evolution performance of g-C₃N₄ is remarkably enhanced and the H₂ evolution rate reaches 2.3 μmol h⁻¹. The photocatalytic activity of the Ag₂S/g-C₃N₄ composites further increases with increasing AgS content from 2 to 5%, and the maximum activity is observed at 5% Ag₂S/g-C₃N₄, with H₂ evolution rate reaches 10 μmol h⁻¹, about 100 times higher than that of pure g-C₃N₄. A further increase in the content of Ag₂S leads to a reduction of the photocatalytic activity for 10% Ag₂S/g-C₃N₄ sample with H₂-production rate of 3.9 μmol h⁻¹. This is probably due to the fact that excessive Ag₂S covered on the surface of g-C₃N₄ could shield the incident light, which inhibits the formation of enough photogenerated carriers. It should be noted that no H₂ can be detected when Ag₂S alone was used as the catalyst, suggesting that pure Ag₂S is not active for photocatalytic H₂ production. We also tested the photocatalytic activity of Pt/g-C₃N₄ composite (1% wt Pt) under the same conditions. Unexpectedly, the as-prepared Pt/g-C₃N₄ composite show almost no photocatalytic H₂ production activity, which is quite different from other pure g-C₃N₄, prepared from the cyanamide or dicyanamide precursor.^{12,34} This result indicates that the g-C₃N₄ prepared from the urea precursor show poor photocatalytic H₂ production activity under the current tested condition, which indirectly highlights the unique co-catalyst function of Ag/Ag₂S.

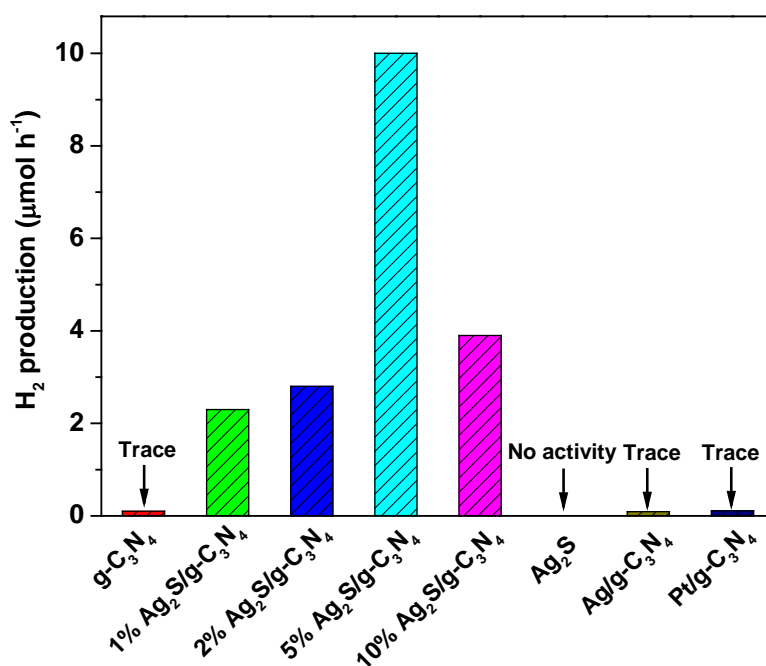


Fig. 7 Comparison of the photocatalytic H₂ evolution activity of Ag₂S/g-C₃N₄ composites as well as pure g-C₃N₄, Ag₂S, Ag/g-C₃N₄, and 1.0wt% Pt/g-C₃N₄ samples from 25% methanol aqueous solution (20 mL methanol + 60 mL distilled water under visible light irradiation (12 W, 420 nm).

Notably, it can be found from the time course of H₂ evolution (shown in Fig. S2) that, all of the amounts of H₂ evolution over the composite catalysts do not appear as linear functions of the reaction time in the tested hours. If examined closely, the data points collected at the end of the first hour fall below where they should appear on the lines. This unusual results infer that pure Ag₂S alone is not the effective cocatalyst for the H₂ evolution of g-C₃N₄. After reaction for one hour, however, the amounts of H₂ evolution for the composite samples increase rapidly, almost appearing as linear functions of the reaction time. We thus assume that another cocatalyst may contribute to this significant increase in the amounts of H₂ evolution. To confirm this point, we first conducted the recycle experiments over the 5% Ag₂S/g-C₃N₄ sample. As shown in Fig. 8a, in the second, third and fourth cycle, the amounts of H₂ evolution appears as linear functions of the reaction time, although a slight decrease in the activity was observed after the second cycle. This

decrease trend was essentially inhibited in the third and fourth cycles, revealing that the Ag/Ag₂S/g-C₃N₄ ternary photocatalyst has the good photostability. To check the phase of the final sample, XRD analysis was then carried out on the 5% Ag₂S/g-C₃N₄ sample after four times recycle experiments. The XRD pattern in Fig. 8b shows that some new diffraction peaks which can be indexed to the Ag appears, indicating that a part of Ag₂S nanoparticles were reduced to Ag either by the reduction of photogenerated electron or the visible light irradiation. The diffraction peaks ascribed to the g-C₃N₄ are the same for the fresh and used photocatalysts, implying the high stability of g-C₃N₄. This result implies that Ag/Ag₂S formed by the simultaneous photoreduction in the first cycle most probably acts as the cocatalyst for the g-C₃N₄ in the following cycles. Further, is the Ag nanoparticles responsible for the H₂ evolution? To exclude the effect of Ag nanoparticles on the H₂ evolution of g-C₃N₄, we thus synthesized the Ag/Ag₂S sample (see Supporting Information) and test its H₂ evolution activity under the same condition. The results shows that Ag/Ag₂S sample has a negligible visible light H₂-production activity (Fig. 7). Thereby, it is reasonable to conclude that the Ag/Ag₂S formed by the simultaneous photodeposition likely contributes to the effective H₂ evolution of g-C₃N₄.

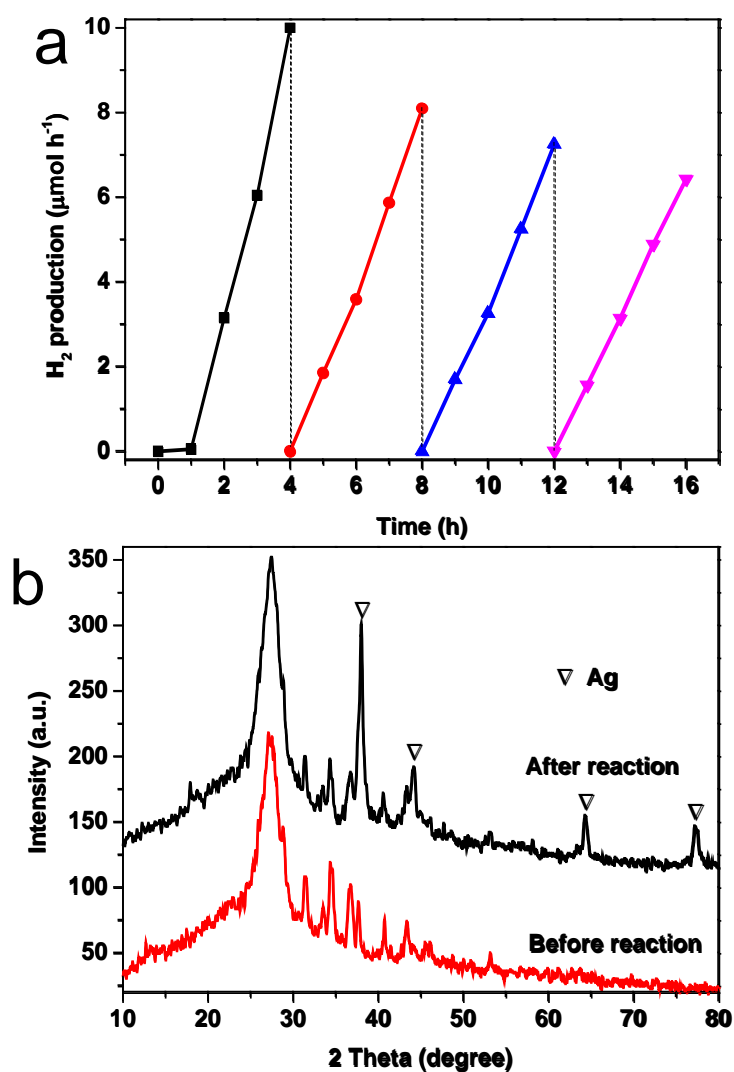


Fig. 8 (a) Cycling runs for the photocatalytic H₂ evolution in the presence of 5% Ag₂S/g-C₃N₄ composite under visible light irradiation. (b) XRD patterns of the 5 % Ag₂S/g-C₃N₄ sample before and after the fourth cycle.

3.5 Possible Photocatalytic Mechanism

On the basis of the above-mentioned results, a possible mechanism for the enhanced H₂ evolution activity of Ag₂S/g-C₃N₄ is tentatively proposed and was shown in Fig. 9. Although the conduction band (CB) edge of g-C₃N₄ is more negative than the reduction potential of H⁺/H₂, the rate of H₂ production was negligible over single g-C₃N₄ in the absence of Ag₂S due to the rapid

recombination rate of CB electrons and valence band (VB) holes. However, after Ag_2S modification, the photocatalytic H_2 production activity of $\text{g-C}_3\text{N}_4$ is readily evoked. Since the CB level of Ag_2S is lower than the CB of $\text{g-C}_3\text{N}_4$, the photoexcited electron from the $\text{g-C}_3\text{N}_4$ CB can transport electrons to Ag_2S . Due to the low H_2 production activity, we infer that such electron transfer is slow, as displayed in Fig. 9a. However, it should be noted that at the beginning, the transferred electrons from $\text{g-C}_3\text{N}_4$ CB to Ag_2S may cause the reduction of partial Ag^+ to Ag^0 . The formed Ag nanoparticle thus acts as a sink for photogenerated electrons, which could promote the separation and transfer of photo-generated electrons from the $\text{g-C}_3\text{N}_4$ CB to the $\text{Ag}/\text{Ag}_2\text{S}$, where H^+ is reduced to hydrogen molecules (Fig. 9b). As a result, H_2 production activity of the $\text{g-C}_3\text{N}_4$ with the assistance of $\text{Ag}/\text{Ag}_2\text{S}$ was greatly enhanced.

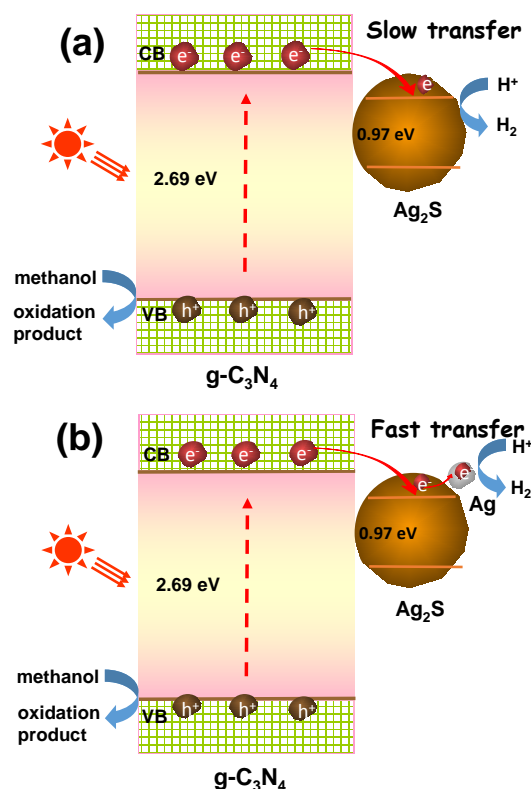


Fig. 9 Proposed mechanism for photocatalytic H_2 -production over $\text{g-C}_3\text{N}_4$ in the presence of Ag_2S

(a) and $\text{Ag}/\text{Ag}_2\text{S}$ (b).

To justify the above assumption, we used photoluminescence (PL) spectroscopy to analyse

the extent of the charge separation of the photocatalysts, and the results are shown in Fig.10. The main emission peak centers at about 460 nm for the pure $g\text{-C}_3\text{N}_4$ sample, which can be ascribed to the band gap recombination of electron-hole pairs. Compared with $g\text{-C}_3\text{N}_4$, addition of Ag_2S does not alter the spectral position of the peaks, but reduces the relative intensity of PL spectral. As expected, once Ag are formed on the Ag_2S surface by the simultaneous photodeposition, the photoluminescence further drops markedly. We interpret the reduction of total photoluminescence yield as an indication of the efficient transfer of photoexcited electrons between $g\text{-C}_3\text{N}_4$ and $\text{Ag}/\text{Ag}_2\text{S}$. Overall, it can be drawn a conclusion that $\text{Ag}/\text{Ag}_2\text{S}$ behaves in a similar manner to Pt, accepting and transferring electrons and functioning as an effective hydrogen evolution promoter for $g\text{-C}_3\text{N}_4$.

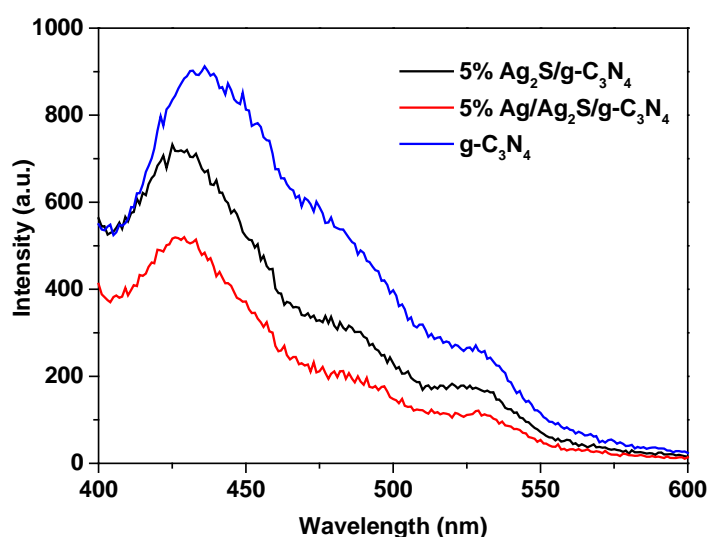


Fig. 10 Room temperature PL spectra of $g\text{-C}_3\text{N}_4$, 5% $\text{Ag}_2\text{S}/g\text{-C}_3\text{N}_4$, and 5% $\text{Ag}/\text{Ag}_2\text{S}/g\text{-C}_3\text{N}_4$ under the excitation wavelength of 330 nm.

Our result was similar to the previously reported results.⁵⁷⁻⁵⁹ For example, Yu and co-worker recently found that $\text{Cu}(\text{OH})_2$ cluster can act as a very efficient co-catalyst for the photocatalytic H_2 -production of TiO_2 .⁵⁸ They found that at the beginning of the photocatalytic reaction, the

transferred electrons from TiO₂ CB to Cu(OH)₂ clusters will cause the reduction of partial Cu²⁺ to Cu⁰ atoms, resulting in the formation of Cu clusters. These Cu clusters can work as a co-catalyst to promote the separation and transfer of photo-generated electrons from the TiO₂ CB to the Cu(OH)₂/Cu cluster, where H⁺ is reduced to hydrogen molecules. Such phenomenon was also found in the Ni(OH)₂/TiO₂ system, where a few of simultaneously formed Ni⁰ particles performed as the co-catalyst.⁵⁹ In the present work, the Ag/Ag₂S composite formed by the simultaneous photoreduction probably acts as the electron sink to help the charge separation and as the cocatalyst for water reduction, thus enhancing the photocatalytic H₂-production activity.

4. Conclusion

Ag₂S-modified graphitic carbon nitride (Ag₂S/g-C₃N₄) composite photocatalysts were successfully prepared via a simple precipitation method. The photocatalytic H₂-production activity of g-C₃N₄ can be greatly increased by the combination of Ag₂S. The 5% Ag₂S/g-C₃N₄ composite gives a H₂ production of 10 μmol h⁻¹, around 100 times that of pure g-C₃N₄ and 1.0wt% Pt/g-C₃N₄. The photocatalytic mechanism study highlights that, the Ag/Ag₂S, which is formed by simultaneous photodeposition in the photocatalytic H₂ evolution reaction, could act as the efficient co-catalyst for the photocatalytic H₂ production of g-C₃N₄. The enhanced activity can be ascribed to the effective separation and fast multistep transfer of photogenerated charges originating from the formation of Ag/Ag₂S/g-C₃N₄ ternary composite with contacted heterojunction interfaces. This finding showed the possibility for the utilization of Ag₂S or Ag/Ag₂S a substitute for Pt in the photocatalytic H₂ production using g-C₃N₄ or other photocatalyst.

Acknowledgements

This work was supported by the financial supports of National Natural Science Foundation of

China (21003065), Jiangsu Planned Projects for Postdoctoral Research Funds (1202040C), College Natural Science Research Program of Jiangsu Province (13KJB610003), Zhenjiang Industry Supporting Plan (GY2013023) and Zhenjiang Social Developing Plan (SH2013002) and Research Foundation for Talented Scholars of Jiangsu University (11JDG149 and 10JDG133).

Notes and references

Electronic Supplementary Information (ESI) available: [Plot of $(\alpha h\nu)^{1/2}$ versus energy ($h\nu$) for the band gap energy of g-C₃N₄ and the plot of $(\alpha h\nu)^2$ versus energy ($h\nu$) for the band gap energy of Ag₂S. Time course of H₂ evolution over Ag₂S/g-C₃N₄ composites as well as pure g-C₃N₄ and Ag₂S samples. Synthetic procedures, TEM image and XRD pattern of Ag/g-C₃N₄ composite. Measured N₂ sorption parameters of the samples].

- [1] A. Fujishima and K. Honda, *Nature*, 1972, **238**, 37.
- [2] U. A. Joshi, A. Palasyuk, D. Arney, and P. A. Maggard, *J. Phys. Chem. Lett.*, 2010, **1**, 2719.
- [3] Z. G. Zou and H. Arakawa. *J. Photochem. Photobio A*, 2003, **158**, 145.
- [4] R. V. D. Krol, Y. Q. Liang and J. Schoonman, *J. Mater. Chem.*, 2008, **18**, 2311.
- [5] X. Zong, H. J. Yan, G. P. Wu, G. J. Ma, F. Y. Wen, L. Wang and C. Li, *J. Am. Chem. Soc.*, 2008, **130**, 7176.
- [6] B. Chai, T. Y. Peng, P. Zeng, X. H. Zhang and X. J. Liu, *J. Phys. Chem. C*, 2011, **115**, 6149.
- [7] K. Maeda and K. Domen, *J. Phys. Chem. C*, 2007, **111**, 7851.
- [8] Z. Wang, J. G. Hou, C. Yang, S. Q. Jiao, K. Huang and H. M. Zhu, *Energy Environ. Sci.*, 2013, **6**, 2134.
- [9] J. Zhang, J. G. Yu, Y. M. Zhang, Q. Li and J. R. Gong, *Nano Lett.*, 2011, **11**, 4774.
- [10] Y. X. Li, G. Chen, Q. Wang, X. Wang, A. K. Zhou and Z. Y. Shen, *Adv. Funct. Mater.*, 2010,

20, 3390.

- [11] A. Kudo and Y. Miseki, *Chem. Soc. Rev.*, 2009, **38**, 253.
- [12] X. C. Wang, K. Maeda, A. Thomas, K. Takanabe, G. Xin, J. M. Carlsson, K. Domen and M. Antonietti, *Nat. Mater.*, 2009, **8**, 76.
- [13] Y. Wang, X. C. Wang and M. Antonietti, *Angew. Chem. Int. Ed.*, 2012, **51**, 68.
- [14] Y. Zheng, J. Liu, J. Liang, M. Jaroniec and S. Z. Qiao, *Energy Environ. Sci.*, 2012, **5**, 6717.
- [15] J. H. Sun, J. S. Zhang, M. W. Zhang, M. Antonietti, X. Z. Fu and X. C. Wang, *Nat. Commun.*, 2012, **3**, 1139.
- [16] J. Xu, Y. J. Wang and Y. F. Zhu, *Langmuir*, 2013, **29**, 10566.
- [17] Y. W. Zhang, J. H. Liu, G. Wu and W. Chen, *Nanoscale*, 2012, **4**, 5300.
- [18] G. H. Dong and L. Z. Zhang, *J. Mater. Chem.*, 2012, **22**, 1160.
- [19] S. C. Yan, Z. S. Li and Z. G. Zou, *Langmuir*, 2010, **26**, 3894.
- [20] Y. Wang, Y. Di, M. Antonietti, H. R. Li, X. F. Chen and X. C. Wang, *Chem. Mater.*, 2010, **22**, 5119.
- [21] G. Liu, P. Niu, C. Sun, S. C. Smith, Z. Chen, G. Q. (Max) Lu and H. Cheng, *J. Am. Chem. Soc.*, 2010, **132**, 11642.
- [22] Y. Wang, Y. Di, M. Antonietti, H. R. Li, X. F. Chen and X. C. Wang, *Chem. Mater.*, 2010, **22**, 5119.
- [23] J. S. Zhang, X. F. Chen, K. Takanabe, K. Maeda, K. Domen, J. D. Epping, X. Z. Fu, M. Antonietti and X. C. Wang, *Angew. Chem. Int. Ed.*, 2010, **49**, 441.
- [24] J. S. Zhang, G. G. Zhang, X. F. Chen, S. Lin, L. Möhlmann, G. Dołęga, G. Lipner, M. Antonietti, S. Blechert and X. C. Wang, *Angew. Chem. Int. Ed.*, 2012, **51**, 3183.

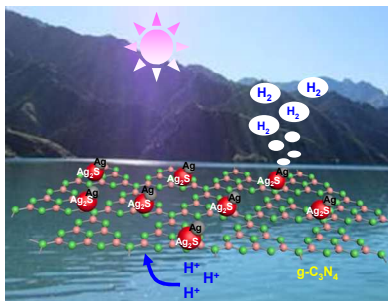
- [25] G. G. Zhang and X. C. Wang, *J. Catal.*, 2013, **307**, 2463.
- [26] L. Ge, F. Zuo, J. K. Liu, Q. Ma, C. Wang, D. Z. Sun, L. Bartels and P. Y. Feng, *J. Phys. Chem. C*, 2012, **116**, 13708.
- [27] L. Ge, C. C. Han, X. L. Xiao and L. L. Guo, *Appl. Catal. B: Environ.*, 2013, **142–143**, 414.
- [28] X. X. Xu, G. Liu, C. Random and J. T. S. Irvine, *Int. J. Hydrogen. Energy*, 2011, **36**, 13501.
- [29] X. J. Bai, R. L. Zong, C. X. Li, D. Liu, Y. F. Liu and Y. F. Zhu, *Appl. Catal. B: Environ.*, 2014, **147**, 82.
- [30] Q. J. Xiang, J. G. Yu and M. Jaroniec, *J. Phys. Chem. C*, 2011, **115**, 7355.
- [31] L. Ge, C. C. Han, X. L. Xiao and L. L. Guo, *Int. J. Hydrogen. Energy*, 2011, **36**, 13501.
- [32] D. L. Jiang, L. L. Chen, J. J. Zhu, M. Chen, W. D. Shi and J. M. Xie, *Dalton Trans.*, 2013, **42**, 15726.
- [33] D. L. Jiang, J. J. Zhu, M. Chen and J. M. Xie, *J. Colloid Interface Sci.* 2014, **417**, 115.
- [34] Y. Di, X. C. Wang, A. Thomas and M. Antonietti, *ChemCatChem*, 2010, **2**, 834.
- [35] B. Chai, T. Y. Peng, J. Mao, K. Li and L. Zan, *Phys. Chem. Chem. Phys.*, 2012, **14**, 16745.
- [36] J. G. Yu, S. H. Wang, B. Cheng, Z. Lin and F. Huang, *Catal. Sci. Technol.*, 2013, **3**, 1782.
- [37] X. Zong, J. F. Han, G.J. Ma, H. J. Yan, G. P. Wu and C. Li, *J. Phys. Chem. C*, 2011, **115**, 12202.
- [38] Y. D. Hou, A. B. Laursen, J. S. Zhang, G. G. Zhang, Y. S. Zhu, X. C. Wang, S. Dahl and I. Chorkendorff, *Angew. Chem. Int. Ed.*, 2013, **52**, 3621.
- [39] J. D. Hong, Y. S. Wang, Y. B. Wang, W. Zhang and R. Xu, *ChemSusChem*, 2013, **6**, 2263.
- [40] K. Nagasuna, T. Akita, M. Fujishima and H. Tada, *Int. J. Hydrogen. Energy*, 2011, **27**, 7294.
- [41] K. Nagasuna, T. Akita, M. Fujishima and H. Tada, *Langmuir*, 2011, **27**, 7294.

- [42] I. Hwang and K. Yong, *ChemPhysChem*, 2013, **14**, 364.
- [43] Y. X. Li, G. Chen, C. Zhou and J. X. Sun, *Chem. Commun.*, 2009, **15**, 2020.
- [44] R. Vogel, P. Hoyer and H. Weller, *J. Phys. Chem.*, 1994, **98**, 3183.
- [45] S. Liu, X. T. Wang, W. X. Zhao, K. Wang, H. X. Sang and Z. He, *J. Alloys Comp.*, 2013, **568**, 84.
- [46] S. H. Shen, L. J. Guo, X. B. Chen, F. Ren, S. S. Mao, *Int. J. Hydrogen. Energy*, 2010, **35**, 7110.
- [47] J. Fu, B. B. Chang, Y. L. Tian, F. N. Xi and X. P. Dong, *J. Mater. Chem. A*, 2013, **1**, 3083.
- [48] G. Liao, S. Chen, X. Quan, H. Yu and H. Zhao, *J. Mater. Chem.*, 2012, **22**, 2721.
- [49] T. Thongtema, A. Phuruangrat and S. Thongtem, *Mater. Lett.*, 2010, **64**, 136.
- [50] A. Thomas, A. Fischer, F. Goettmann, M. Antonietti, J. O. Muller, R. Schlogl and J. M. Carlsson, *J. Mater. Chem.*, 2008, **18**, 4893.
- [51] Y. Q. Sun, C. Li, Y. X. Xu, H. Bai, Z. Y. Yao and G. Q. Shi, *Chem. Commun.*, 2010, **46**, 4740.
- [52] Y. S. Xu and W. D. Zhang, *ChemCatChem*, 2013, **5**, 2343.
- [53] D. Chandra, K. Saito, T. Yui, and M. Yagi. *Angew. Chem. Int. Ed.*, 2013, **52**, 1.
- [54] J. P. Xiao, Y. Xie, R. Tang and W. Luo, *J. Mater. Chem.*, 2002, **12**, 1148.
- [55] L. L. Chen, D. L. Jiang, T. He, Z. D. Wu and M. Chen, *CrystEngComm*, 2013, **15**, 7556.
- [56] Z. D. Meng, T. Ghosh, L. Zhu, J. G. Choi, C. Y. Park and W. C. Oh, *J. Mater. Chem.*, 2012, **22**, 16127.
- [57] P. Gomathisankar, D. Yamamoto, H. Katsumata, T. Suzuki and S. Kaneco, *Int. J. Hydrogen. Energy*, 2013, **38**, 5517.

[58] J. G. Yu and J. R. Ran, *Energy Environ. Sci.*, 2011, **4**, 1364.

[59] J. G. Yu, Y. Hai, and B. Cheng, *J. Phys. Chem. C*, 2011, **115**, 4953.

Graphical Abstract



Novel $\text{Ag}_2\text{S}/\text{g-C}_3\text{N}_4$ composite photocatalysts with efficient Pt-free hydrogen evolution activity were fabricated. The $\text{Ag}/\text{Ag}_2\text{S}$, formed by simultaneous photodeposition in the photocatalytic H_2 evolution reaction, were found to act as an efficient co-catalyst for the photocatalytic H_2 production of $\text{g-C}_3\text{N}_4$.